ISSN 1027-5495. Functional Materials, 27, No.1 (2020), p. 107-116.
doi:https://doi.org/10.15407/fm27.01.107

Cobalt based coatings as catalysts for methanol oxidation

T.A.Nenastina, M.V.Ved', N.D.Sakhnenko, I.Yu.Yermolenko, M.Volobuyev, V.O.Proskurina

National Technical University "Kharkiv Polytechnic Institute",
2 Kyrpychova Str., 61002 Kharkiv, Ukraine

Received September 23, 2019

The cobalt based coatings with refractory metals (Mo, W, Zr) were deposited from pyrophosphate-citrate electrolytes in a pulsed mode. It has been shown that, with increasing current density, Co–Mo–W and Co–W–ZrO_2 alloys are enriched in tungsten, grain sizes decrease, but a network of cracks appears on the surface of the Co–Mo–W coating. In the Co–Mo–ZrO_2 coating, with increasing current density, the zirconium content increases due to molybdenum, and the surface is the most fractured and small-globular. The surface roughness parameters for Co–Mo–ZrO_2 are one order of magnitude higher than those for Co–Mo–W. Cyclic voltammograms show that the Co–Mo–ZrO_2 deposits are characterized by the highest stability under anodic polarization due to the inclusion of molybdenum and zirconium(IV) oxide in their composition. The kinetics of the methanol anodic oxidation on electrodes coated with cobalt alloys was studied, and the participation of intermediate metal oxides in oxygen transport was revealed. A significant increase in the anode current peak indicates a higher electro-catalytic activity of the zirconium-containing coatings among the studied alloys.

Keywords: cobalt based alloys, electrodeposition, pulse electrolysis, catalytic activity, methanol anodic oxidation.

Покрытия сплавами кобальта с тугоплавкими металлами (Mo, W, Zr) получены из пирофосфатно-цитратных электролитов в импульсном режиме. Показано, что с ростом плотности тока сплавы Co–Mo–W и Co–W–ZrO_2 обогащаются вольфрамом, размеры зерен уменьшаются, однако на поверхности покрытия Co–Mo–W появляется сетка трещин. В покрытии Co–Mo–ZrO_2 с ростом плотности тока увеличивается содержание циркония за счет молибдена, причем поверхность является наиболее трещиноватой и мелкоглобулярной. Параметры шероховатости поверхности Co–Mo–ZrO_2 на порядок выше, чем для Co–Mo–W. Циклические вольтамперограммы показывают, что сплавы Co–Mo–ZrO_2 характеризуются самой высокой стабильностью при анодной поляризации благодаря включению в их состав оксидов молибдена и циркония. Исследована кинетика анодного окисления метанола на электродах с покрытиями тройными сплавами, выявлено участие промежуточных оксидов металлов в переносе кислорода. Существенный рост тока анодного пика свидетельствует о более высокой среди изученных сплавов электрокаталитической активности цирконийсодержащих покрытий.

Покриття на основі кобальту як каталізатори електроокиснення метанолу. *Т.О.Ненастіна, М.В.Ведь, М.Д.Сахненко, І.Ю.Єрмоленко, М.М.Волобуєв, В.О.Проскуріна.*

Покриття сплавами кобальту з тугоплавкими металами (Mo, W, Zr) осаджені з пірофосфатно-цитратних електролітів в імпульсному режимі. Показано, що з ростом густини струму сплави Co–Mo–W і Co–W–ZrO_2 збагачуються вольфрамом, розміри зерен зменшуються, проте на поверхні покриття Co–Mo–W з'являється сітка тріщин. У покритті Co–Mo–ZrO_2 з підвищенням густини струму збільшується вміст цирконію за рахунок молібдену, причому поверхня є найбільш тріщинуватою і дрібноглобулярною. Параметри шорсткості Co–Mo–ZrO_2 на порядок вищі, ніж для Co–Mo–W. Циклічні

вольтамперограми показують, що сплави Co–Mo–ZrO_2 характеризуються найвищою стабільністю при анодній поляризації завдяки включенню до їх складу оксидів молібдену і цирконію. Досліджено кінетику анодного окислення метанолу на електродах з покриттями сплавами кобальту, виявлено участь проміжних оксидів металів у перенесенні оксигену. Істотне зростання струму анодного піка свідчить про більш високу серед вивчених сплавів електрокаталітичну активність цирконійвмісних покриттів.

1. Introduction

The development of efficient power supply sources (PSS) has always been and remains to be one of the most promising areas that ensure energy stability of any country. A wide range of PPSs also includes fuel cells (FC), considered as the most ecologically safe and promising energy sources, because the reactions therein are reduced to the formation of water from the fuel, in particular, hydrogen and oxygen [1–3]. A sticking point of FC is electrode materials which act as catalytic agents. In the vast majority of cases, these are expensive materials related to the platinum and silver family [4–6]. In addition to their high electrocatalytic activity, such materials differ by their stability and chemical resistance in the media of different mineralization and corrosiveness. Earlier researches [7–11] showed that transition metal-based alloys can be decent competitors to precious metals.

Lately, the researches of new types of fuel for FC, such as methanol, ethanol, formaldehyde, and hydrocarbons, have found many applications [12]. Liquid fuels, such as low molecular alcohols, have certain advantages in comparison with pure hydrogen because these are easy-to-store and transport. Moreover, their energy capacity is comparable with the energy capacity of usual liquid fuels (gasoline, kerosene, etc.), for example, it is 6 KW/kg for methanol.

The obtained research data show that different organic substances are reversibly oxidized on platinum family metals at relatively low anode potentials. The electrocatalytic oxidation mechanism and the products also depend on the electrode material [13]. Today, platinum is considered as one of the best catalysts of the electrooxidation of monoatomic alcohols. However, much attention is paid to the development of less expensive materials that can replace platinum [14]. The main requirements to the catalysts are reduced to three properties: high catalytic activity, chemical and corrosion resistance, and nontoxicity. Undoubtedly, the activity of catalysts is defined by the material nature, though it depends to a great extent on the surface condition. It is known that molybdenum compounds possess a certain catalytic activity with regard to many processes, for example, electrochemical methanol oxidation, the reduction of iodates, etc. [15]. Cobalt compounds, such as oxides and complexes, are also used in electrocatalysis [16]. Evidently, it is related to the mobility of oxygen contained in the compounds of metals, their high coordination capacity, and ability to form nonstoichiometric oxides [17].

The use of alkaline electrolytes allows us to extent the range of materials that can be used for the formation of catalytic matrices. It is due to the acceleration of the reduction reactions of oxygen and simple alcohols in alkaline electrolytes in comparison with acid electrolytes, and a lower corrosiveness of the former with regard to many transition metals. The problems of the use of methanol as a fuel in the alkaline environment are related to a gradual carbonization of the electrolyte when alcohol is oxidized to CO_2, and poisoning the precious metal-based electrodes. Transition metal alloys and manganese oxides turned out to be efficient catalysts that reduce the poisoning effect [18, 19]. Hence, studying the mechanism of the methanol oxidation on such alloys as well as the maintenance of phasic oxidation with no formation of carbon dioxide can become a highly promising approach to the replacement of precious metals by more economic catalytic systems.

Hence, the formation of the layer of electrolytic alloys based on cobalt with molybdenum (tungsten), and zirconium that has a branched globular surface can provide a preset route for the methanol electrooxidation process and increase the FC operation efficiency using no precious metals. The subject of this paper is studying:

— the influence of the electrolysis conditions and the nature of the doping components (molybdenum, tungsten, zirconium) on the surface morphology, catalytic activity and resistance of coatings to anodic oxidation in an alkaline medium;

— the participation of intermediate oxides as products of the incomplete reduction of oxometallates in methanol oxidation process.

Table. Effect of the current density i and pulse/pause duration (t_{on}/t_{off}) on the composition of the ternary cobalt coatings

Specimen #	Electrolyte composition, mol/dm^3	Electrolysis parameters		Composition (in the terms of metal)*, wt.%
		i, A/dm^2	t_{on}/t_{off}, ms	
1 (Co–Mo–W)	$CoSO_4$ — 0.2, Na_2WO_4 — 0.16 Na_2MoO_4 — 0.08	4	2/10	Co — 59.94, Mo — 23.28, W — 16.77
2 (Co–Mo–W)		6	2/10	Co — 61.0, Mo — 20.6, W — 18.4
3 (Co–Mo–ZrO_2)	$CoSO_4$ — 0.15	4	2/10	Co — 62.1, Mo — 33.3, Zr — 4.6
4 (Co–Mo–ZrO_2)	Na_2MoO_4 — 0.06	4	5/10	Co — 63.6, Mo — 32.6, Zr — 3.8
5 (Co–Mo–ZrO_2)	$Zr(SO_4)_2$ — 0.05	6	5/10	Co — 69.0, Mo — 26.6, Zr — 4.4
6 (Co–W–ZrO_2)	$CoSO_4$ — 0.15, Na_2WO_4 —0.06, $Zr(SO_4)_2$ — 0.05	4	2/10	Co — 88.2, W — 9.1, Zr — 2.7
7 (Co–W–ZrO_2)		6	2/10	Co — 73.8, W — 24.4, Zr — 1.8

* The content of oxygen in deposited coatings, wt.%: Co–Mo–W — 12–15; Co–Mo–ZrO_2 — 10–12; Co–W–ZrO_2 — 6–10; due to incomplete reduction of oxometalates and incorporation of intermediate oxides in the alloys matrix.

2. Experimental

The electrolytic methanol oxidation mechanism was investigated using electrodes with electrolytic coatings of Co–Mo–W, Co–Mo–ZrO_2, and Co–W–ZrO_2 alloys of at least 5 μm thick. The coatings were deposited from the biligand pyrophosphate-citrate electrolytes [9, 20] (with the following compositions: 0.1 mol/dm^3 of $K_4P_2O_7$ for Co–Mo–(W)ZrO_2 and 0.4 mol/dm^3 of $K_4P_2O_7$ for Co–Mo–W; 0.2 mol/dm^3 of $Na_3C_6H_5O_7$ and 0.5 mol/dm^3 of Na_2SO_4) with addition of metal compounds; the deposition was carried out onto the steel substrate (Table). The solutions were prepared from chemically pure reagents using distilled water. The samples were subjected to the preliminary treatment using the methods given in [21]. The electrodeposition was conducted using the pulse current at a varied current density, and on/off time ratios [9, 20]. The electrolyte temperature at a level of 30–35°C was maintained.

The chemical composition of the coatings was determined by energy dispersive X-ray spectroscopy using an Oxford INCA Energy 350 electron probe microanalyzer integrated into the SEM system. X-rays were excited by exposure of the samples to a beam of 15 keV electrons. The surface morphology of the deposits was studied with a Zeiss EVO 40XVP scanning electron microscope (SEM). Images were made by registering secondary electrons (SEs) under scanning with an electron beam; this mode made it possible to study the topography with a high resolution and contrast ratio.

The surface relief and morphology of the 10×10×2 mm^3 samples were evaluated by the contact method with an NT-206 scanning probe AFM microscope (lateral and vertical resolutions are 2 and 0.2 nm, respectively; 1024×1024 scanning matrix; a CSC cantilever as a probe, the probe tip radius being 10 nm) [22–24].

The polarization plots were obtained for Co–Mo–W(ZrO_2) electrodes using a potentiostat PI-501.1 and the programmer PR-8 equipped with the special device intended for the digital data registration. Cyclic voltammetry data (CV) were analyzed at the potential scanning rates s of 0.002 V/s to 0.05 V/s according to the algorithm given in [25]. A standard three-electrode cell was used for the measurements, a platinum spiral served as an auxiliary electrode, and a saturated silver-chloride reference electrode was connected to the cell via a salt bridge. The electrolytes of 0.25 M NaOH, and 0.25 M NaOH + 1 M CH_3OH compositions were prepared using pure reagents and distilled water.

3. Results and discussion

The coatings formed by ternary Co–Mo–W alloys (Table, specimens 1, 2) are characterized by the uniformly branched globular surface whose relief differs considerably from that of the substrate one (Fig. 1, a, b).

We can see the cracks and a number of pores on the surface of the specimen 2 (Fig. 2) which is coated with Co–Mo–W at the current density of 6 A/dm^2. This phenomenon can be explained by two reasons. First, a higher rate of nucleation and

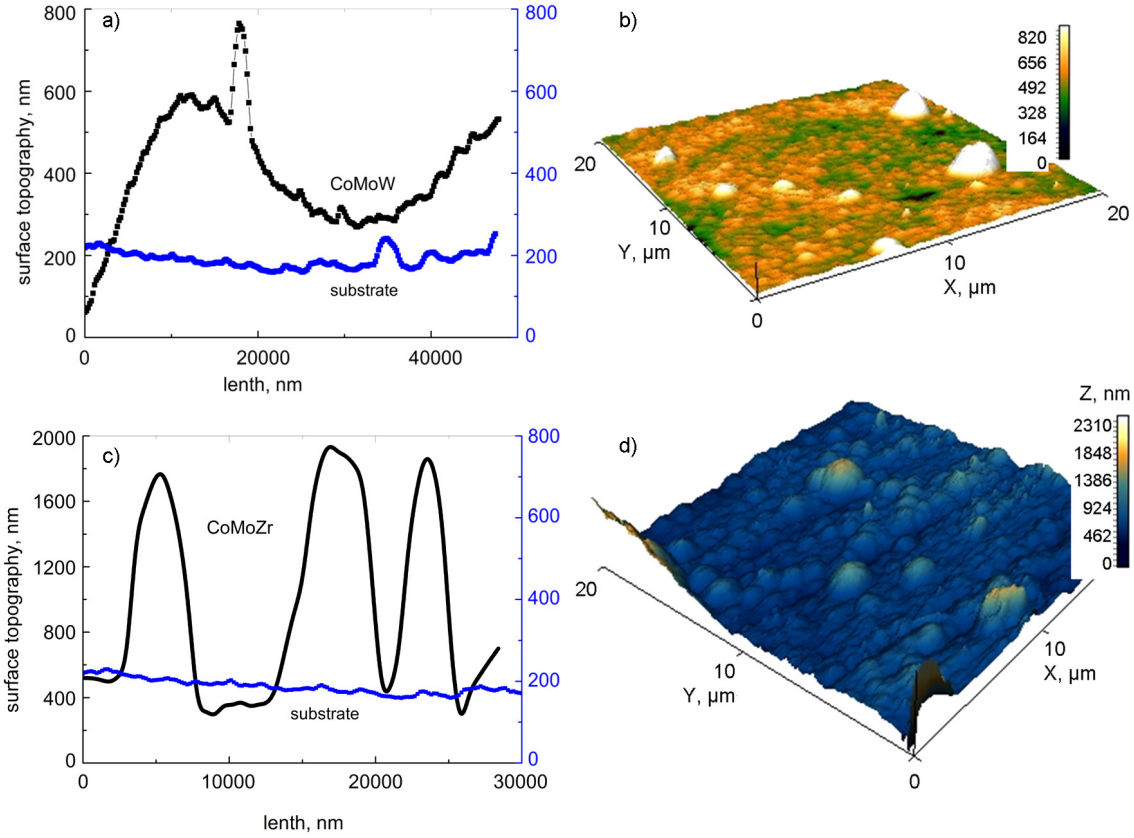

Fig. 1. Topography (a, b) and the relief (c, d) of the surface of Co–Mo–W alloy (Specimen 1 Table (a, b) and Co–Mo–ZrO_2 alloy (specimen 3, Table (c, d).

growth of crystallites at a higher current density leads to an increase in internal stresses in the coating and following cracking. Second, the hydrogen evolution reaction is intensified with increasing polarization, and causes the porosity of the coating.

The analysis of AFM data is indicative of the nano-globular character of the surface of the Co–Mo–W coatings; cone-shaped aggregates with the diameter of 2 to 5 μm are formed due to the merging of fine globules with the diameter of 20 to 80 nm. The roughness parameters calculated for the section area of 20×20 μm are: $R_a = 0.02$ and $R_q = 0.04$.

The Co–Mo–ZrO_2 ternary coatings differ from the Co–Mo–W ones by a more branched surface, and uniformly distributed cone-shaped aggregates with the diameter of 5 to 7 μm (Fig. 1, c, d). The cobalt content increases with the current density and an extension of the pulse time. However, the percentage of doping metals is decreased in comparison with that of Co–Mo–W coatings (Table, specimens 3–5). At the same time, ceteris paribus, with increasing current density, the zirconium content slightly increases (Table, specimens 4 and 5). Despite this, the origination of cracks in the Co–Mo–ZrO_2 coatings is independent of the refractory components content as well as of current density. Many studies paid attention to the cracking of binary and ternary cobalt and molybdenum alloys [26, 27]. A possible cause of the coatings fracturing may be the difference in the crystalline lattice types of the doping metals. It is known that the cobalt and zirconium crystal structure is hexagonal close packed (hcp), while molybdenum and tungsten are characterized by a body-centered cubic (bcc) crystalline lattice.

The analysis of the AFM data obtained for the Co–Mo–ZrO_2 coatings on the 20×20 μm section allowed us to calculate the roughness parameters of R_a and R_q as 0.1 and 0.2, respectively; they are one order of magnitude higher than those for the Co–Mo–W coatings.

The morphology and relief of the Co–W–ZrO_2 coatings are similar to those of the Co–Mo–W ones (Fig. 2, specimens 6, 7); however, the tungsten content is smaller in the alloys obtained under the same electrolysis conditions (Table, specimens 1 and

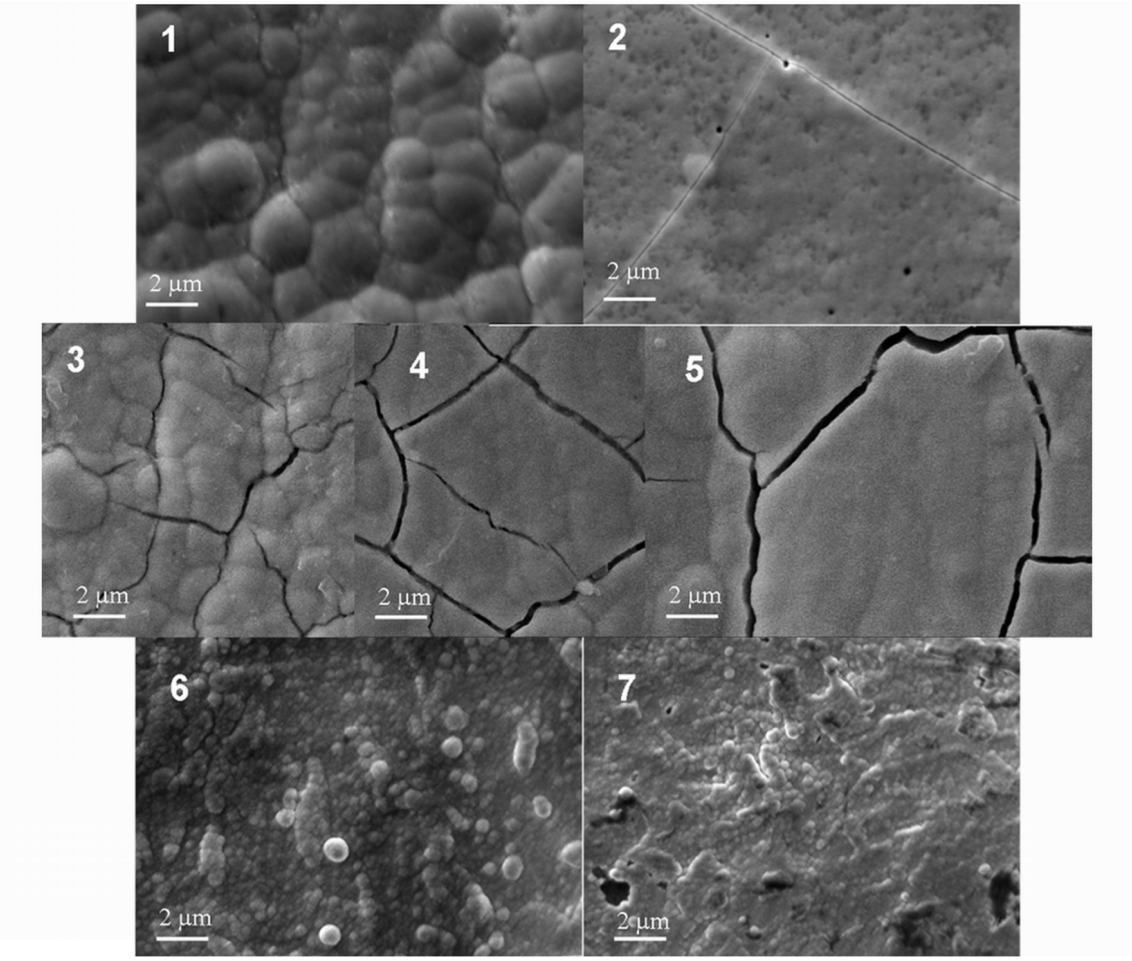

Fig. 2. Morphology of the ternary cobalt coatings surface (SEM photo, magnification × 5000). The number of specimens corresponds to that in the Table.

2). It should be noted that zirconium percentage in the Co–W–ZrO_2 coatings is also lower in comparison to that in the Co–Mo–ZrO_2 ones deposited under the same conditions (Table, specimens 3 and 5). A decrease in the size of agglomerates and the absence of the cracks in the coatings might be related to the influence of tungsten on the electro-crystallization process. An increase in the current density contributes to the tungsten enrichment of the coating, though the content of zirconium reduces to 1.8 wt% (Table, specimens 6 and 7).

Nevertheless, as shown in [21, 28–30], the relief and a surface development degree of all the coatings mentioned above are favorable for the catalytic processes occurring not only through the adsorption stage but also in the diffusion. It is evident that the difference in the surface structure and morphology of the electrolytic alloys will have an effect on their electrochemical behavior, in particular on the catalytic activity in electrode reactions, namely, methanol anodic oxidation.

A complete methanol oxidation is a multistage process that can be represented as a series of stages:

$$(CH_3OH)_L \rightarrow (CH_3OH)_S \rightarrow \quad (1)$$
$$\rightarrow (HCHO)_S \rightarrow (HCOO^-)_S \rightarrow (CO)_S \rightarrow CO_2.$$

Here $()_L$ are the particles in the solution, $()_S$ are intermediate products and the particles adsorbed by the electrode surface.

The given series fails to reflect the whole process mechanism, because in addition to the solution components, intermediate metal oxides that are formed on the catalyst electrode surface during the anode polarization can participate in it. In this case, the reversibility of the processes that occur on the electrodes is the precondition for the efficient operation of the catalysts.

Let's consider the individual stages of the electrode process and detect the specific features of each stage. The first stage of

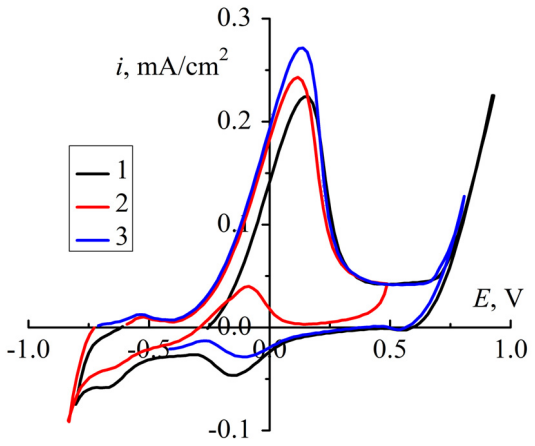

Fig. 3. Cyclic voltamograms of methanol oxidation on platinum nail electrode. Numbers of the cycle are 1, 2, and 3.

the adsorption of methanol molecules on the electrode surface that corresponds to the $(CH_3OH)_L \rightarrow (CH_3OH)_S$ transformation can limit the electrode process only in the case of fast and completely reversible single-stage charge transfer in the electrochemical reaction. It is known that the oxidation of organic molecules is not of that type; therefore, we can conclude that the adsorption process is reversible with regard to the charge transfer stage. The second stage, $(CH_3OH)_S \rightarrow (HCHO)_S$, is directly related to the charge transfer, and it is electrochemical. The methanol oxidation that results in the formation of aldehyde is accompanied by the hydrogen atom and carbon σ-bond rupture, and the formation of the double bond between carbon and oxygen:

$$(CH_3OH)_S + 2OH^- \rightarrow \rightarrow (HCHO)_S + 2H_2O + 2e. \quad (2)$$

Particularly this stage is considered to be limiting, and its rate can be controlled by the system cycling without carbon dioxide formation and solution carbonization. The conduction of the process in the interval of potentials that corresponds to the given stage is an essential and sufficient condition for the control of the entire oxidation process.

The next stage of methanol oxidation conducted to get methane acid is also electrochemical, and it is related to the substitution of hydrogen atom by oxygen one according to the gross-scheme:

$$((HCHO)_S\} + 3OH^- \rightarrow \rightarrow (HCHO^-)_S + 2H_2O + 2e. \quad (3)$$

A degree of the reversibility of this stage depends on the lability of oxygen atoms whose donor can be the hydroxide ions that are present in the solution. However, it is more probable that the surface oxides of the electrode material that are formed during the anode polarization will participate in this stage. For example, according to the transfer reaction of oxygen atom from the metal oxide MO_x to carbon:

$$(HCHO)_S + (MO_x)_S \rightarrow \rightarrow (HCOOH)_S + (MO_{x-1})_S, \quad (4)$$

the reaction is transformed into the chemical one, and as a consequence, the process probability and the rate of it on the whole are increased. It is evident that the catalytic activity of the alloys of cobalt, molybdenum, and tungsten (zirconium) is explained particularly by a high donor-acceptance capacity with regard to oxygen and the formation of oxides of a variable composition on the alloy surface during the anode polarization:

$$(MO_{x-1})_S + 2OH^- \rightarrow (MO_x)_S + H_2O + 2e. \quad (5)$$

Oxygen in them is mobile and can be transferred to the carbon atom without additional energy inputs as in the case of the participation of hydroxide ions in the reaction (3).

Subsequent transitions in the anodic process are related to the formation of a water molecule and intermediate carbon oxide (II) according to the chemical reaction:

$$(HCOOH)_S \rightarrow (CO)_S + H_2O, \quad (6)$$

a further $(CO)_S \rightarrow CO_2$ transformation is of no interest for the functioning of fuel cells, and this link can be excluded from the general scheme, as long as the potential varying intervals are limited.

Hence, the investigation of the process of methanol oxidation on the alloys of cobalt with molybdenum and tungsten (zirconium) is the foundation for the formation of efficient catalysts for FC. Electro-catalytic properties of the Co–Mo–W and Co–Mo(W)–ZrO_2-coated electrodes were studied in the model methanol oxidation reaction using the method of cyclic voltammetry (CV); the obtained data were compared with those for the electrochemical behavior of

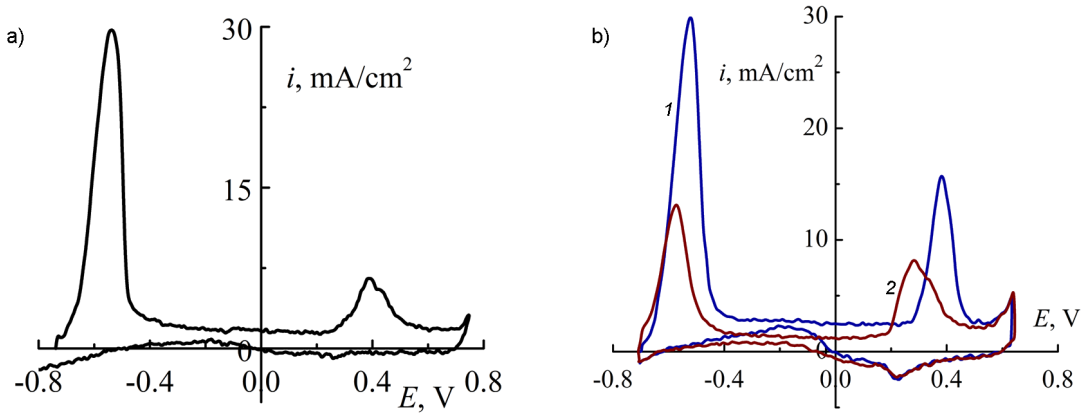

Fig. 4. Cyclic voltamograms of Co–Mo–W-coated electrodes (specimen 1) in the 0.25 M NaOH solution (a) and in the presence of methanol (b).

the platinum electrode in the analogous solution (Fig. 3), and with the CV data of cobalt based alloys in the background solution of 0.25 M NaOH.

The CV for the platinum electrode shows that one peak of the methanol oxidation is displayed at the half-peak potential of $E_{pa/2}$ (from –0.05 V to 0.0 V), the current peak is 0.25 mA/cm^2, and the inverse peak is actually two times lower than the direct anode peak. The difference between the potentials of oxidation half-peaks $E_{pa/2}$ and the inverse peak of $E_{pc/2}$ is within 30 mV that is indicative of anode reaction to be quasi-reversibility, and it progresses with the participation of two electrons (stage 2). The anodic polarization of the Pt electrode in the second cycle (plot 2 in Fig. 3) was specially switched to the opposite after the peak was visualized, but before oxygen evolution began. The goal was to show that methanol oxidation on platinum occurs in at least two stages, and the peak potential of the reverse stroke just corresponds to the potential of a direct half-peak: from –0.05 V to 0 V. It means that adsorbed intermediate aldehyde is oxidized to an acid. This is not observed if the anodic polarization reaches potentials greater than +0.7 V when CO_2 is a dominant product.

The anodic CV plots obtained for ternary Co–Mo–W and Co–Mo–ZrO_2 alloys in the 0.25 M NaOH solution show the peak at the potentials of (0.35–0.4) V that can be related to the oxidation of alloy components to form the intermediate oxides. The peak current on the Co–Mo–W-coated electrodes is within 7.0 to 7.5 mA/cm^2, and it is one order of magnitude higher than the current for the Co–Mo–ZrO_2 electrode (Fig. 4a, 5a). However, the coatings are characterized by chemical resistance and a tendency to passivity in the alkaline solution.

On the CV plots for Co–Mo–W-coated electrodes in the presence of methanol (Fig. 4b, plot 1) the anode peak current i_p of the first cycle is shifted to the side of lower potentials ($E_{pa/2}$ = 0.22 to 0.24 V) in comparison with the data for the 0.25 M NaOH solution ($E_{pa/2}$= 0.35 to 0.37 V), and the peak current increases to 9.0–9.5 mA/cm^2 that is indicative of the surface oxides participation in the methanol oxidation reaction. Moreover, the difference between the peak currents in the background solutions and in the presence of methanol is in the range of 2.0–2.2 mA/cm^2. It exceeds the methanol oxidation current on the platinum electrode (see Fig. 3) that confirms the catalytic properties of the alloy. In the second cycle of the polarization, the potential's half-peak returns to the level peculiar for the background solution, and the peak current is increased twice. In this case, the cycling results do not change in the general pattern. This behavior can be explained by the presence of intermediate oxides of doping metals, which are formed in the anodic process and reduced during the inverse polarization; i.e. the mechanism suggested in this paper that includes the stages (4) and (5) is realized.

A comparative analysis of the CV plots shows that the activity of the Co–Mo–ZrO_2-coated electrodes in the methanol oxidation reaction is considerably higher than that of Co–Mo–W and platinum, because the oxidation peak current is higher by a factor of 2.0 to 2.5 (Fig. 5). Such an increased efficiency of the electrodes can be explained by a higher degree of the surface branching (see Fig. 1) and a synergetic effect of the metals, such as cobalt, molybdenum, and zirconium, which are characterized by dif-

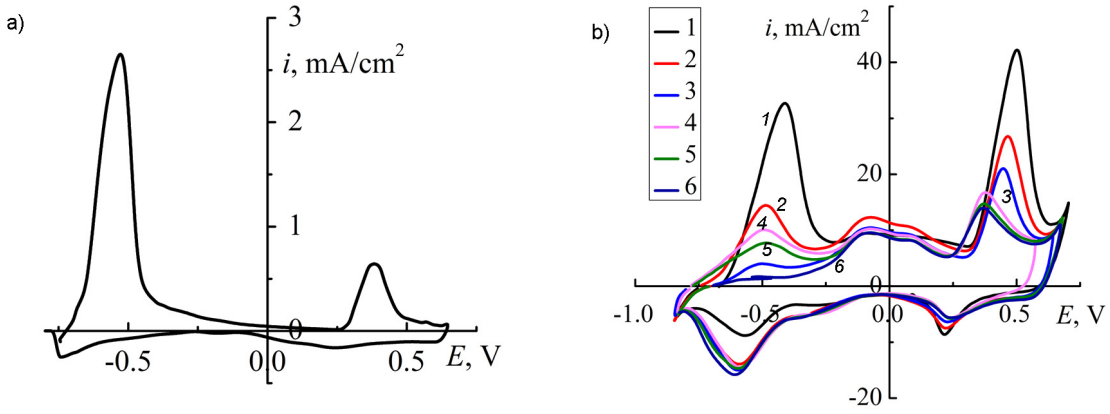

Fig. 5. Cyclic voltamograms for $Co–Mo–ZrO_2$ coated electrodes (specimen 3) in 0.25 M NaOH solution (a) and in the presence of methanol (b).

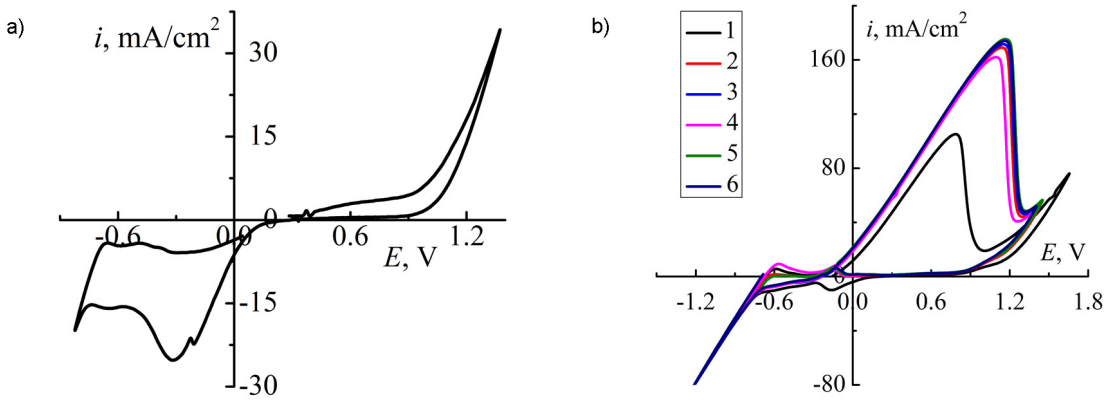

Fig. 6. Cyclic voltamograms of $Co–W–ZrO_2$ coated electrodes (specimen 6) in 0.25 M NaOH solution (a) and in the presence of methanol (b).

ferent degrees of the stability to oxidation and affinity to oxygen [8, 9, 20].

It should be noted that the oxidation waves of methanol on the alloys are symmetric relative to i_p. It confirms the availability of the adsorption stage and is indicative of the reaction quasi-reversibility. The oxidation peak current is increased in the range from the first cycle to the second cycle; then it is decreased and stabilized at the level of 16 mA/cm^2 to 18 mA/cm^2 in the fifth cycle. The half-peak anode potentials decrease; this is indicative of a decrease in the overpotential. Starting from the second cycle, the inverse behavior of the CV plot is actually not changed, i.e. the process becomes more stable, and as for the Co–Mo–W-coated electrode, it progresses according to the stages (4) and (5).

A peculiarity of the electrochemical behavior of the $Co–W–ZrO_2$ coated electrodes in the background alkaline solution is unavailability of the peak on the anode branch of the CV, and the origination of a broad peak of the cathode reduction (Fig. 6a).

The type of the CV characteristic is changed abruptly in the presence of methanol; a sloping broad peak appears during the anode polarization, and the inverse peak disappears, which is indicative of the irreversibility of anode process (Fig. 6, b). The current peak is increased in the range from the first cycle to the fourth one; afterwards it is slightly decreased and stabilized at the level of 160–165 mA/cm^2, which is almost one order of magnitude higher than for the $Co–Mo–ZrO_2$ coated electrodes. Considering an increase in the slope of an ascending branch of the anodic polarization dependence and absence of the inverse peak, we can conclude that the process on the electrodes is irreversible, and a strong current is related to the simultaneous oxidation of coating components and methanol. In addition, it should be taken into consideration that the $Co–W–ZrO_2$ coatings have a more branched surface in comparison with the series of the alloys in question.

From the CV analysis, we can make a conclusion that the electrolytic Co–Mo–ZrO_2 alloy can be considered as the most promising in terms of catalytic activity in the reversible cyclic process, though Co–Mo–W and Co–W–ZrO_2 alloys can be used for noncyclic processes. Thus, electrodes coated with Co–Mo–ZrO_2 alloy can be considered as the most promising for electrocatalysis [31].

4. Conclusions

The Co–Mo–W(ZrO_2) coatings with the total content of refractory metals of 30–40 wt.%, and Co–W–ZrO_2 alloys with that of 12–26 wt.% were deposited from pyrophosphate-citrate electrolytes by pulse current. A uniformly developed cone-shaped surface of the coatings is due to tungsten and molybdenum incorporation, but the molybdenum containing ternary coatings differs by the network of shallow cracks.

Anodic behavior of the Co–Mo(W)–ZrO_2 coatings in the alkali solution is associated with formation of doping metals oxides during anodic polarization and their quasi-reversible reduction, and indicates higher stability of the ternary coatings containing zirconium. Simultaneously, an increase in the cobalt content in the alloy facilitates its passivation in the alkaline medium.

The mechanism and kinetics of anodic methanol oxidation on the electrodes with electrolytic cobalt based alloys is determined. Based on the experiments carried out, we can conclude that the reaction $(CH_3OH)_S \rightarrow (HCOOH)_S$ is the limiting stage, and oxides of doping metals take part in the methanol chemical oxidation being the oxygen donor for intermediate $(HCHO)_S$. The last accelerates the oxidation. The obtained data are indicative of a rather high electrocatalytic activity of the cobalt based alloys, namely Co–Mo–ZrO_2, for methanol oxidation in the alkaline medium. Such catalytic properties can be explained by a higher degree of surface branching and synergetic effect of cobalt, molybdenum, and zirconium which are characterized by variable oxidation states and oxygen affinity.

Hence, a high catalytic activity and chemical stability of the Co–Mo–ZrO_2 coatings allows us to view them as promising electrode materials for chemical current sources, in particular fuel cells.

References

1. I.S.Averkov, A.V.Baykov, L.S.Yanovskiy, V.M.Volokhov, *Russ.Chem.Bull.*, **65**, 2375 (2017).
2. N.V.Korovin, A.S.Sedlov, Y.A.Slavnov et al., *Therm.Eng.*, **54**, 137 (2007).
3. N.M.Mench, Fuel Cell Engines, John Wiley and Sons Inc., New Jersey (2008).
4. L.Liu, A.Corma, *Chem.Rev.*, **118**, 4981 (2018).
5. J.Greeley, J.K.Norskov, M.Mavrikakis, *Annu. Rev.Phys.Chem.*, **53**, 319 (2002).
6. M.R.Tarasevich, V.A.Bogdanovskaya, in: Electrocatalysts for Low Temperature Fuel Cells: Fundamentals and Recent Trends, ed. by T.Maiyalagan, V.S.Saji, Wiley, VCH Verlag GmbH & Co. KGaA (2017).
7. M.Ved, M.Glushkova, N.Sakhnenko, *Functional Materials*, **20**, 87 (2013).
8. N.D.Sakhnenko, M.V.Ved, Y.K.Hapon, T.A.Nenastina, *Russ.J.Appl.Chem.*, **88**, 1941 (2015).
9. G.Yar-Mukhamedova, M.Ved', N.Sakhnenko, T.Nenastina, *Appl.Surf.Sci.*, **445**, 298 (2018).
10. M.V.Ved', M.A.Koziar, N.D.Sakhnenko, M.A.Slavkova, *Functional Materials*, **23**, 420 (2016).
11. Y.S.Yapontseva, A.I.Dikusar, Y.S.Kyblanovskii, *Surf.Eng.Appl.Electrochem.*, **50**, 330 (2014).
12. V.VPoplavskii, T.S.Mishchenko, V.G.Matys, *Tech.Phys.*, **55**, 296 (2010).
13. A.E.Wendlandt, S.S.Stahl, *Angew.Chem.Int. Ed.Engl.*, **54**, 14638 (2015).
14. J.Zhang, L.Shangguan, S.Shuang et al., *Russ. J.Electrochem.*, **49**, 888 (2013).
15. C.Song, M.Khanfar, P.Pickup, *J.Appl.Electrochem.*, **36**, 339 (2006).
16. Y.Pirskyy, N.Murafa, O.Korduban et al., *J. Appl.Electrochem.*, **44**, 1193 (2014).
17. V.Baklan, M.V.Uminsky, I.P.Kolesnikova, in: Fuel Cell Technologies: State and Perspectives., ed. by N.Sammes, A.Smirnova, O.Vasylyev, Springer, Dordrecht (2005).
18. J.Zeng, J.Y.Lee, *J.Power Sources*, **140**, 268 (2005).
19. J.Fei, L.Sun, C.Zhou et al., *Nanoscale Res. Lett.*, **12**, 23 (2017).
20. M.V.Ved', N.D.Sakhnenko, I.Y.Yermolenko, T.A.Nenastina, in: Nanochemistry, Biotechnology, Nanomaterials, and their Applications, ed. by O.Fesenko, L.Yatsenko, Springer, Cham (2018).
21. M.V.Ved', M.D.Sakhnenko, O.V.Bohoyavlens'ka, T.O.Nenastina, *Mater.Sci.*, **44**, 79 (2008).
22. G.Yar-Mukhamedova, N.Sakhnenko, M.Ved' et al., *IOP Conf. Ser.: Mater. Sci. Engin.*, **213** (2017).
23. M.V.Ved', M.D.Sakhnenko, H.V.Karakurkchi et al., *Mater.Sci.*, **51**, 701 (2016).
24. I.Y.Yermolenko, M.V.Ved', N.D.Sakhnenko, Y.I.Sachanova, *Nanoscale Res.Lett.*, **12**, 352 (2017).
25. D.Thomas, Z.Rasheed, J.S.Jagan, K.G.Kumar, *J.Food Sci.Technol.*, **52**, 6719 (2015).

26. P.N.S.Casciano, L.Ramon, R.L.Benevides, R.A.C.Santana, *J. Alloys Compd.*, **723**, 164 (2016).
27. V.S.Kublanovsky, Y.S.Yapontseva, *Electrocatal*, **5**, 372 (2014).
28. M.Ved, N.Sakhnenko, T.Bairachnaya, N.Tkachenko, *Functional Materials*, **15**, 613 (2008).
29. I.Y.Yermolenko, M.V.Ved', N.D.Sakhnenko et al., *Functional Materials*, **25**. 274 (2018).
30. R.Yakushin, K.Kuterbekov, D.Grafov et al., *Safety in Technosphere*, **3**, 40 (2015).
31. V.Shemet, J.Piron-Abellan, W.Quadakkers, L.Singheiser, in: Fuel Cell Technologies: State and Perspectives, ed. by N.Sammes, A.Smirnova, O.Vasylyev, Springer, Dordrecht (2005).